

RESEARCH ARTICLE

Two different isoforms of osteopontin modulate myelination and axonal integrity

Gisela Nilsson¹  | Amin Mottahedin¹  | Aura Zelco¹  | Volker M. Lauschke^{2,3,4}  |
 C. Joakim Ek¹  | Juan Song^{1,5} | Maryam Ardalan¹  | Sha Hua^{1,6} | Xiaoli Zhang^{1,5}  |
 Carina Mallard¹  | Henrik Hagberg⁷  | Jianmei W. Leavenworth^{8,9}  |
 Xiaoyang Wang^{1,5,7} 

¹Centre of Perinatal Medicine & Health, Department of Physiology, Institute of Neuroscience and Physiology, Sahlgrenska Academy, University of Gothenburg, Gothenburg, Sweden

²Department of Physiology and Pharmacology, Karolinska Institute, Stockholm, Sweden

³Dr Margarete Fischer-Bosch Institute of Clinical Pharmacology, Stuttgart, Germany

⁴University of Tübingen, Tübingen, Germany

⁵Henan Key Laboratory of Child Brain Injury, Institute of Neuroscience and Third Affiliated Hospital of Zhengzhou University, Zhengzhou, China

⁶Department of Cardiology, Ruijin Hospital/Luwan Branch, School of Medicine, Shanghai Jiao Tong University, Shanghai, China

⁷Centre of Perinatal Medicine & Health, Department of Obstetrics and Gynaecology, Institute of Clinical Sciences, Sahlgrenska Academy, University of Gothenburg, Gothenburg, Sweden

⁸Department of Neurosurgery, University of Alabama at Birmingham, Birmingham, Alabama, USA

⁹Department of Microbiology, University of Alabama at Birmingham, Birmingham, Alabama, USA

Correspondence

Jianmei W. Leavenworth, Department of Neurosurgery, University of Alabama at Birmingham, Birmingham, AL 35233, USA.

Email: jleavenworth@uabmc.edu

Xiaoyang Wang, Centre of Perinatal Medicine & Health, Department of Obstetrics and Gynaecology, Institute of Clinical Sciences, Sahlgrenska Academy, University of Gothenburg, Box 432, SE-405 30 Gothenburg, Sweden.

Email: xiaoyang.wang@fysiologi.gu.se

Funding information

Swedish Research Council, Grant/Award Number: 2019-01837, 2016-

Abstract

Abnormal myelination underlies the pathology of white matter diseases such as preterm white matter injury and multiple sclerosis. Osteopontin (OPN) has been suggested to play a role in myelination. Murine OPN mRNA is translated into a secreted isoform (sOPN) or an intracellular isoform (iOPN). Whether there is an isoform-specific involvement of OPN in myelination is unknown. Here we generated mouse models that either lacked both OPN isoforms in all cells (OPN-KO) or lacked sOPN systemically but expressed iOPN specifically in oligodendrocytes (OLs-iOPN-KI). Transcriptome analysis of isolated oligodendrocytes from the neonatal brain showed that genes and pathways related to increase of myelination and altered cell cycle control were enriched in the absence of the two OPN isoforms in OPN-KO mice compared to control mice. Accordingly, adult OPN-KO mice showed an increased axonal myelination, as revealed by transmission

Abbreviations: CTNNA1, α -catenin; DEGs, differentially expressed genes; ECM, extracellular matrix; eNOS, endothelial nitric oxide synthase; GO, Gene Ontology; KEGG, Kyoto Encyclopedia of Gene and Genomes; MACS, magnetic-activated cell sorting; MBP, myelin basic protein; mTORC1, mTOR complex 1; NRG, neuregulin; OPCs, oligodendrocyte precursors; OPN, osteopontin; P, postnatal day; PCA, principal component analysis; PLP1, myelin proteolipid protein 1; PTGER2, prostaglandin E receptor 2; RNA-seq, RNA-sequencing; RT-qPCR, reverse transcription-quantitative PCR; Spp1, secreted phosphoprotein 1; TCF7L2, transcription factor 7-like 2; TEM, transmission electron microscopy.

This is an open access article under the terms of the [Creative Commons Attribution-NonCommercial-NoDerivs](https://creativecommons.org/licenses/by-nc-nd/4.0/) License, which permits use and distribution in any medium, provided the original work is properly cited, the use is non-commercial and no modifications or adaptations are made.

© 2023 The Authors. *FASEB BioAdvances* published by Wiley Periodicals LLC on behalf of The Federation of American Societies for Experimental Biology.

01154, 2016-01153, 202101872, 2019-01320, 2021-01950, 2018-02682 and 2015-06276; Brain Foundation, Grant/Award Number: FO2019-0056 and FO2017-0102; Swedish Government, Grant/Award Number: ALFGBG-966107, ALFGBG-432291, ALFGBG-966034, ALFGBG-813291 and ALFGBG-429801; National Natural Science Foundation of China, Grant/Award Number: 81771418; W o M Lundgren, Grant/Award Number: 3126-2019, 1804-2017 and 1320-2016; Castegrens minne, Grant/Award Number: LA2016-0404; Goljes minne, Grant/Award Number: LA2015-0255; Mary von Sydow, Grant/Award Number: 3618 and 4617; Åhlénstiftelsen, Grant/Award Number: mH3h18 and 193054; Elisabeth “Bollan” Lindén; Swedish Strategic Research Programme in Diabetes (SFO Diabetes); Stem Cells and Regenerative Medicine (SFO StratRegen); Chinese Scholarship Council, Grant/Award Number: 201407040032; Health Commission of Henan Province, Grant/Award Number: 2018069; Henan Administration of Foreign Experts Affairs, Grant/Award Number: 2019023

electron microscopy imaging, and increased expression of myelin-related proteins. In contrast, neonatal oligodendrocytes from OLs-iOPN-KI mice compared to control mice showed differential regulation of genes and pathways related to the increase of cell adhesion, motility, and vasculature development, and the decrease of axonal/neuronal development. OLs-iOPN-KI mice showed abnormal myelin formation in the early phase of myelination in young mice and signs of axonal degeneration in adulthood. These results suggest an OPN isoform-specific involvement, and a possible interplay between the isoforms, in myelination, and axonal integrity. Thus, the two isoforms of OPN need to be separately considered in therapeutic strategies targeting OPN in white matter injury and diseases.

KEYWORDS

myelin, oligodendrocytes, osteopontin isoforms, RNA-sequencing

1 | INTRODUCTION

Oligodendrocytes are the myelinating cells of the central nervous system (CNS). The inability of oligodendrocytes to myelinate axons underlies the pathology of white matter diseases such as preterm white matter injury and multiple sclerosis. The primary cellular target in preterm white matter injury is premyelinating oligodendrocytes that are abundantly present in the brain during weeks 23–32 of gestation in humans and at postnatal day (P) 2–7 in mice.¹ Oligodendrocytes at this developmental stage are especially vulnerable to insults such as infection and inflammation, and the identification of factors that regulate normal oligodendrocyte development and myelination is essential for understanding the mechanisms underlying white matter injury and disease.

Osteopontin (OPN), encoded by the secreted phosphoprotein 1 (*Spp1*) gene, is a multifunctional glycoposphoprotein involved in various physiological and pathological processes.^{2–5} The diverse functions of OPN are attributable to its multiple variants arising from transcriptional, posttranscriptional, and posttranslational modifications. An alternative translation of the OPN

mRNA generates two isoforms of OPN, a secreted form (sOPN) and an intracellular form (iOPN).^{6,7} Although most functional activities of OPN have been ascribed to sOPN, accumulating evidence suggests that iOPN also serves specific roles in controlling cell migration, motility, proliferation, and immunity.^{7–15}

OPN expression is frequently upregulated in the CNS under various pathological conditions such as inflammation,¹⁶ neurodegeneration,^{17,18} and perinatal brain injury.^{19–22} We recently showed a marked increase in OPN protein expression in microglia and astrocytes in post-mortem preterm infant brains with white matter injury.²³ In addition, strong OPN immunoreactivity is detected in axons at the periphery of the ischemic zone in both subacute and chronic periventricular leukomalacia lesions in human infants.²⁴

OPN has been suggested to play a role in myelination.^{25,26} It has also been implicated in the pathogenesis of adult white matter diseases,²⁷ and lack of OPN significantly reduces the disease severity of experimental autoimmune encephalomyelitis, an animal model of multiple sclerosis.²⁸ While OPN appears to have adverse effects in some disease models, effects appear to be

context and age dependent as administration of recombinant OPN reduces the infarct size in a murine stroke model²⁹; while in immature brain injury models, OPN either show protection,^{20,21} or does not affect gray or white matter injury following hypoxia-ischemia-induced brain injury.^{19,30} Whether the different outcomes result from the effects of different OPN isoforms and their expression by specific cell types is unknown. In the current study, we generated mouse models that either lacked both OPN isoforms in all cell types (OPN-KO) or lacked sOPN systemically but expressed iOPN specifically in oligodendrocytes (OLs-iOPN-KI) to discern the effects of sOPN and oligodendrocyte-specific iOPN on myelination.

2 | MATERIALS AND METHODS

2.1 | Mice

C57/BL/6J (wild type, Charles River), B6;129S4-*Olig1^{tm1(cre)Rth}/J* (*Olig1^{Cre}*, The Jackson Laboratory), and C57/BL/6J-*Spp1^{flstop/flstop}* (*Spp1^{flstop/flstop}*, Harvey Cantor's laboratory, Dana-Farber Cancer Institute, Boston, MA, USA)⁹ mice were housed and bred at the Experimental Biomedicine facility (University of Gothenburg, Sweden). Animal experiments conformed to the guidelines established by the Swedish Board of Agriculture (SJVFS 2019: 9), were approved by the Gothenburg Animal Ethics Committee (ethical number 2042/18), and were reported in accordance with the ARRIVE guidelines (Animal Research: Reporting of In Vivo Experiments).³¹ Day of birth was defined as post-natal day (P) 0.

2.2 | Immunofluorescent staining of tissue sections

Brains were collected after transcardial perfusion with 0.9% saline followed by Histofix (Histolab, Sweden), and staining was performed on 7- μ m thick sagittal paraffin sections. Immunofluorescent double labeling of Olig2 and OPN was performed on tissue sections from P16 wild type mice ($n=6$ /genotype). After blocking, the sections were incubated with anti-Olig2 (AF2418, R&D Systems, 5 μ g/mL) and anti-OPN (Ab8448, Abcam, 1:250) antibodies followed by incubation with appropriate Alexa Fluor-conjugated secondary antibodies (Invitrogen, 1:500). Mounting was performed using ProLong Gold antifade reagent with DAPI (Invitrogen). Images were acquired using a Zeiss Axio Imager Z2 microscope, and measurements were performed using Fiji ImageJ.

2.3 | Magnetic-activated cell sorting (MACS) of oligodendrocytes

Mice at P5 were decapitated, and the cerebrum brain tissue was collected. Tissue dissociation was performed using the Neural Tissue Dissociation kit (NTDK-P, 130-0292-628, Miltenyi Biotec), a MACSmix tube rotator (130-090-753, Miltenyi Biotec), and a gentle MACS Dissociator (130-093-235, Miltenyi Biotec) according to the manufacturer's instructions. O4⁺ cells were magnetically labeled using Anti-O4 MicroBeads (130-094-543, Miltenyi Biotec) and loaded onto a LS MACS Column (130-042-401, Miltenyi Biotec), which was placed in the magnetic field of a QuadroMACS Separator (130-090-976, Miltenyi Biotec). To increase purity, the O4⁺ cells were applied to a second LS column and the magnetic separation steps were repeated. Cell purity was $\geq 95\%$ as assessed by flow cytometry using the anti-O4 antibody (130-095-887, Miltenyi Biotec) and by immunofluorescent staining.

2.4 | Immunofluorescent staining of cells

MACS-isolated O4⁺ cells from P5 mice were added to a poly-L-lysine (Sigma)-coated chamber slide in culture medium (DMEM:F12-HEPES, 1% penicillin-streptomycin, 0.5% FBS, 30% B104 media, 1 \times B27, and 10 ng/mL FGF-2). Cells were allowed to adhere for 1 h before fixation and permeabilization. After blocking, cells were incubated with primary antibodies (anti-OPN Ab8448, Abcam, 1:250 and anti-Olig2 AF2418, R&D Systems, 5 μ g/mL, or anti-OPN and anti-Calreticulin C6C, Novus Biologicals, 1:500) followed by appropriate Alexa Fluor-conjugated secondary antibodies (Invitrogen, 1:500). Cells were mounted using ProLong Gold antifade reagent with DAPI (Invitrogen), and images were acquired using a Zeiss Axio Imager Z2 microscope.

2.5 | Reverse transcription-quantitative PCR (RT-PCR)

2.5.1 | *Spp1* expression in wild type mouse brain

Mouse brain homogenates at P1, 3, 5, 7, 12, and 16 were prepared ($n=5$ /age). Total RNA was isolated according to the manufacturer's instructions using the miRNeasy Micro Kit (Qiagen). cDNA was prepared using the QuantiTect Reverse Transcription Kit (Qiagen), and PCR

was run on a LightCycler 480 (Roche, Sweden). The following primers were used: *Olig2* QT01041089 and *Spp1* QT00157724. Melting curve analysis was performed to ensure that only one PCR product was obtained. For quantification and for estimation of amplification efficiency, a standard curve was generated using a series of concentrations of cDNA. The amplified *Spp1* transcripts were quantified with the relative standard curve and normalized to the concentration of total cDNA in each sample measured using the Quant-iT™ 338 OliGreen ssDNA Assay Kit 339 (Invitrogen).

2.5.2 | Gene expression in oligodendrocytes

Oligodendrocytes from control-, OPN-KO-, and OLS-iOPN-KI mice ($n=7$) at P5 were isolated using MACS. Total RNA was isolated according to the manufacturer's instructions using the miRNeasy Micro Kit (Qiagen). cDNA was prepared using the QuantiTect Reverse Transcription Kit (Qiagen), and PCR was run on a LightCycler 480 (Roche, Sweden). The following primers were used: *Mbp* QT00198478, *Plp1* QT00096096, *Cnp* QT00106764, and *Mobp* QT00154924. The amplified transcripts were quantified with the relative standard curve and normalized to the concentration of total cDNA in each sample measured using the Quant-iT™ 338 OliGreen ssDNA Assay Kit 339 (Invitrogen).

2.6 | Western blot

Total protein was prepared using mouse brain homogenate, and the protein concentration was determined using a BCA Protein Assay Kit (Sigma). Proteins were separated by SDS-PAGE on a 4%–20% Criterion TGX Stain-Free Precast gels (Bio-Rad). After blotting, the membranes were imaged for total protein. The membranes were incubated with anti-OPN antibody (O-17, IBL, 1:1000), anti-MBP antibody (SMI94, BioLegend, 1:1000), or anti-PLP1 antibody (ab9311, Abcam, 1:1000) followed by HRP-conjugated secondary antibodies (Vector, 1:5000). Enhanced chemiluminescence was performed using the SuperSignal West Dura Extended Duration Substrate (Thermo Scientific), and protein expression levels were quantified using Image Lab (Bio-Rad) and normalized against total protein levels.

2.7 | Transcriptome sequencing and analysis

O4⁺ oligodendrocytes from P5 mouse brains were isolated using MACS ($n=6$ /genotype, both sexes). Total

RNA was isolated according to the manufacturer's instructions using the miRNeasy Micro Kit (Qiagen), and the RNA was sent to Exiqon, Denmark (currently Qiagen), for quality control, library preparation, and RNA-sequencing (RNA-seq) (30M reads, 50bp single-end read). Unsupervised hierarchical clustering and principal component analysis (PCA) of the RNA-seq data were performed using matplotlib in Python. Differential gene expression between control mice and OPN-KO or OLS-iOPN-KI mice was analyzed based on normalized expression data in QluCore Omics Explorer 3.8 (QluCore, Sweden), and multiple tests were accounted for by using the Benjamini-Hochberg correction at a false discovery rate of 0.05. The biological implications of the differentially expressed genes (DEGs) were evaluated using Kyoto Encyclopedia of Gene and Genomes (KEGG) pathway analysis in WebGestalt.³² Gene Ontology (GO) enrichment analysis was performed using g:Profiler (<https://biit.cs.ut.ee/gprofiler/>)³³ and GPlot (1.0.2),³⁴ an R package (R 4.1.1). Regulated molecular pathways and biological functions and diseases were explored by analyzing the DEGs using Ingenuity Pathway Analysis (IPA) (70750971, Qiagen) with a cutoff adjusted p -value of <0.05 . Heatmaps were created using QluCore Omics Explorer 3.8 (QluCore, Sweden).

2.8 | Transmission electron microscopy (TEM)

2.8.1 | 12-week-old mice

Mice ($n=5$) were transcardially perfused with 0.9% saline followed by fixative (0.1 M phosphate buffer pH 7.4, 2.5% glutaraldehyde, and 2% paraformaldehyde) solution. The dissected corpus callosum was postfixed in 1% OsO₄ with 1% K₄Fe(CN)₆ followed by incubation in 0.5% UAC in dH₂O, dehydrated, and gradually infiltrated with acetone: resin at 2:1 and then 1:2 followed by 100% resin and then embedded in 100% resin with accelerator and polymerized at 60°C. The resin was from the Hard Plus Resin 812 kit (EMS). Semi-thin sections (0.5 μm) were stained with Richardson's stain and regions of interest were identified. Ultra-thin sections (70 nm) were stained with lead nitrate and imaged on a Talos L120C TEM. Measurements were performed on three images per animal acquired at 2000× magnification.

2.8.2 | P12 mice

At P12 ($n=5-6$), dissected brain tissue was prepared using the same protocol as for 12-week-old mice except

for using a Leica EM Automatic Microwave Tissue Processor and performing the infiltration at 50°C. For semi-thin sections (0.5 μm), basic fuchsin/azure B staining³⁵ was used, and regions of interest were identified. Ultra-thin sections (70 nm) were stained with lead nitrate and imaged on a Talos L120C TEM. Measurements were performed on six images per animal acquired at 2000 \times magnification.

2.9 | Statistics

GraphPad Prism version 9 (GraphPad software, San Diego, CA, USA) was used to perform the statistical analyses of the RT-PCR, western blot, and structural analysis data. Data were tested for normal distribution through the generation of QQ plots. Data were analyzed using the appropriate test as indicated in the figure legends and presented as bar graphs with mean \pm SD. $p < 0.05$ was considered statistically significant.

3 | RESULTS

3.1 | Generation of OPN knockout (OPN-KO) mice and oligodendrocyte-specific iOPN knock-in (OLs-iOPN-KI) mice

First, we confirmed that OPN is expressed in oligodendrocytes in vivo in brain tissue sections from wild type mice (Figure 1A). In order to investigate a potential isoform-specific involvement of OPN in myelination, we generated OPN-KO and OLs-iOPN-KI mice. We used mice homozygous for the *Spp1*^{flstop} allele knocked into the *Spp1* locus (*Spp1*^{flstop/flstop}). In this system, a STOP cassette is inserted upstream of a mutation site with a deletion of the 45 nucleotides after the translation start site (ATG) that encodes the N-terminal signal sequence directing the secreted form of OPN to the endoplasmic reticulum. Cre/loxP-mediated recombination induces the expression of the iOPN isoform after excision of a STOP

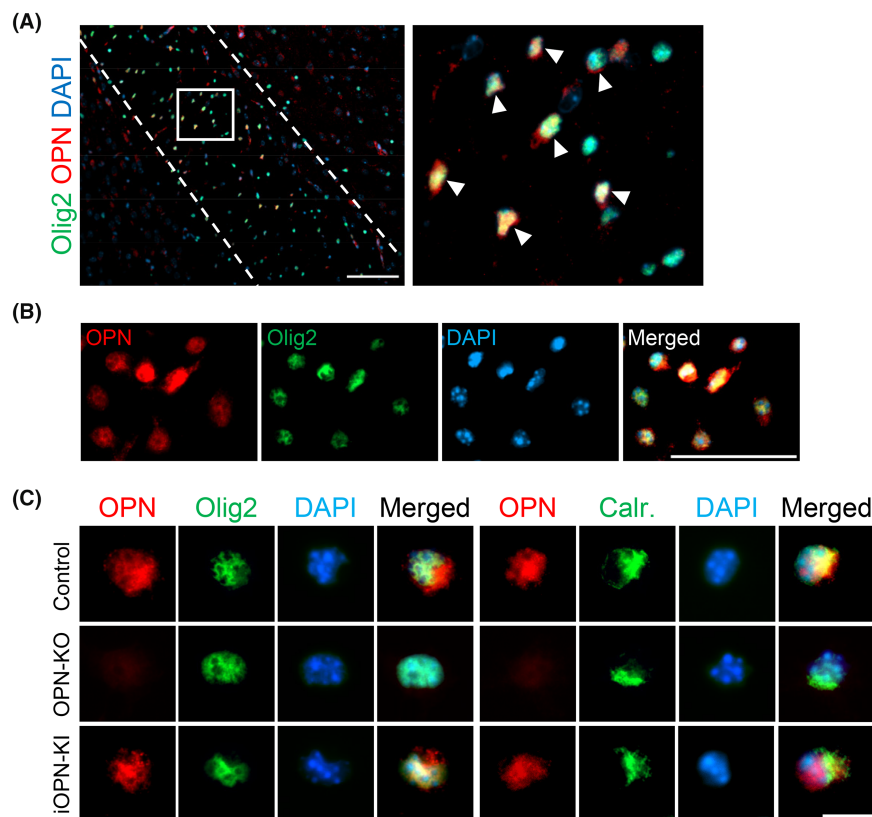


FIGURE 1 Expression of OPN in oligodendrocytes. (A) Left panel: A representative image of fluorescent double staining of Olig2 (green) and OPN (red) with nuclear counterstain (DAPI) in the corpus callosum (delineated area) of wild type mice brain. Right panel: A magnification picture of selected area from the image in the left panel. Arrowheads: Oligodendrocytes expressing OPN. (B) Representative images of O4⁺ oligodendrocytes isolated from control mice at P5, stained using antibodies against OPN (red) and Olig2 (green), and nuclear counterstain (DAPI). (C) Representative images of oligodendrocytes isolated from control, OPN-KO, and OLs-iOPN-KI (iOPN-KI) mice at P5 showing the expression of OPN in oligodendrocytes that were co-stained using antibodies against Olig2 or the endoplasmic reticulum marker calreticulin. Scale bars are 100 μm in (A), 50 μm in (B), and 10 μm in (C).

cassette.⁹ Crossing of *Spp1*^{flstop/flstop} mice with *Olig1*^{Cre} mice^{36,37} generated *Olig1*^{+/+}*Spp1*^{flstop/flstop} (OPN-KO) mice that expressed neither sOPN nor iOPN in any cell type, and *Olig1*^{cre/+}*Spp1*^{flstop/flstop} (hereafter referred to as OLS-iOPN-KI) mice that (1) expressed iOPN specifically in oligodendrocytes; (2) lacked iOPN in all non-oligodendrocyte cell types; and (3) lacked sOPN in all cell types. *Olig1*^{cre/+} *Spp1*^{+/+} mice that expressed both sOPN and iOPN were used as control mice (referred to as control hereafter). The expression of both isoforms in these mice was confirmed by immunofluorescent staining of isolated O4⁺ oligodendrocytes. Analysis of cells from control mice at P5 showed OPN staining in all isolated cells (Figure 1B). Specifically, OPN staining was detected in the endoplasmic reticulum (as marked by calreticulin), suggestive of sOPN, and was also detected in the cytoplasm and nucleus, indicating iOPN (Figure 1C), as reported previously.⁷ In contrast, OPN was not detected in O4⁺ oligodendrocytes isolated from OPN-KO mice, while in the oligodendrocytes isolated from OLS-iOPN-KI mice, OPN staining was mainly detected in the cytoplasm and nucleus and was not substantially stained with calreticulin (Figure 1C).

3.2 | Differential expression of the two OPN isoforms modulates oligodendrocyte gene expression signatures

We first wanted to analyze which genes, biological processes, and signaling pathways in oligodendrocytes were affected by differential expression of the two OPN isoforms. We therefore performed RNA-seq analysis of O4⁺ oligodendrocytes isolated at P5 from control, OPN-KO, and OLS-iOPN-KI mice. Mice at P5 were chosen based on the observation that OPN expression in the brain is highest around this age (Figure S1).¹⁹ Notably,

substantial transcriptomic differences were observed in oligodendrocytes of controls versus OPN-KO or OLS-iOPN-KI mice, while cells from OLS-iOPN-KI mice displayed less distinct segregation compared to OPN-KO cells (Figure 2A). After multiple testing correction ($q < 0.05$), a total of 2609 and 2013 genes were differentially expressed in OPN-KO and OLS-iOPN-KI mice compared to controls, respectively, of which 1108 of the DEGs overlapped between the conditions (Figure 2B). Thus, 1501 genes were differentially expressed specifically in OPN-KO mice, and 905 genes were differentially expressed specifically in OLS-iOPN-KI mice, suggesting specific functional roles of the intracellular and secreted OPN isoforms (Data S1 and S2).

3.3 | Global knockout of both isoforms of OPN leads to gene signatures reflecting increased myelination and altered oligodendrocyte cell cycle control

To examine the effects of the absence of both isoforms of OPN, we focused on the 1501 genes that were differentially expressed specifically in OPN-KO mice (Figure 2B). Among these genes, the top 20 upregulated genes were associated with myelination (*Bcas1*, *Nfe2l3*, *Kif1bp*, and *Bmp4*), cell cycle, proliferation and apoptosis (*Dusp9*, *ErbB3*, and *Tmeff2*), cytoskeleton and cell adhesion (*Cdh7*, *Gipc1*, *Arhgef28*, *Lims2*, and *Tprn*), and metabolism (*B3gnt9*, *Neu4*, and *Mc5r*) (Table S1). The top 20 downregulated genes were linked to cell cycle and apoptosis (*Psrl1*, *Dapk1*, *Ifi204*, *Zfp217*, and *Rel*), neuronal functions (*Lypd6*, *Lrtm*, *Kcnt1*, and *Cacna1h*), inflammation and immunity (*Cybb*, *Cmklr1*, *Rnaset2a*, *Clec4n*, *Rel*, and *Cd36*), and metabolism (*Abhd8*, *Cmklr1*, *Hmox1*, and *Cd36*) (Table S2).

To gain insights into the potential molecular mechanisms involved, we used a systems biology approach to

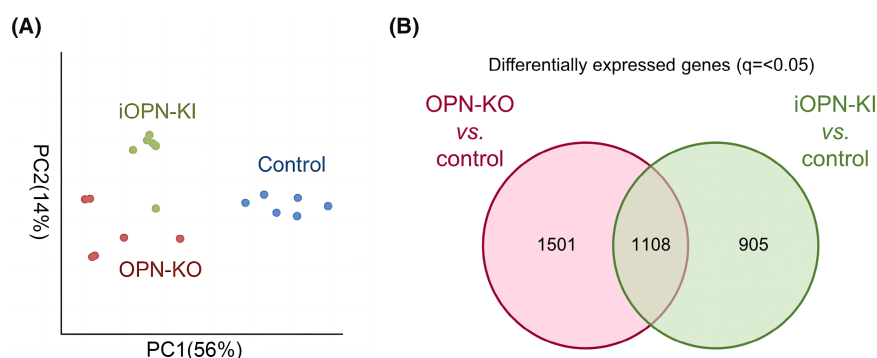


FIGURE 2 Gene expression differences in oligodendrocytes following differential expressions of the two OPN isoforms. Oligodendrocytes were isolated at P5 from control, OPN-KO, and OLS-iOPN-KI mice, and RNA-seq was performed. (A) PCA of the different mouse genotype groups. (B) Venn diagram of DEGs in OPN-KO versus control (pink), OLS-iOPN-KI versus control (green) and overlapping (pink/green).

analyze the biological functions and regulatory pathways underlying the differential gene expression signatures. We first performed IPA core analysis of the 1501 OPN-KO-specific DEGs compared to control ($p < 0.05$, Figure 3A, Data S3). The top predicted increased function was myelination of cells. Accordingly, when focusing on genes implicated in oligodendrocyte development and myelination, we observed upregulation of genes associated with myelination, that is, *Mog*, *Plp1*, *Mag*, *Rtn4*, *Mbp*, *Myrf*, *Cnp*, and *Mopb* in OPN-KO mice (Figure 3B, Data S1 and S2). Gene expression analysis using RT-PCR demonstrated increased expression of *Mbp*, *Plp1*, and *Cnp* in oligodendrocytes of OPN-KO and OLS-iOPN-KI mice compared to control mice, while the expression of *Mopb* was increased in OPN-KO, but not in OLS-iOPN-KI mice (Figure 3C–F). This was in accordance with expression differences observed in the RNA-seq data (Data S1 and S2). Further, significantly enriched biological functions associated with the S phase of cell cycle, viability, survival, and development, including neuronal and vascular development had positive z -scores (Figure 3A). Biological functions that were predicted to be decreased were synthesis of polysaccharides, and functions associated with proliferation and the G2/M cell cycle checkpoint. In addition, significantly enriched biological functions related to cell death and apoptosis had negative z -scores (Figure 3A). Separate analysis of genes involved in cell cycle regulation demonstrated that genes critical for G2/M phase transition and cell cycle progression, for example, *Ccnb1*, *Ccnb2*, *Cdc20*, and *Cdk1*, were downregulated in OPN-KO (Figure 3G, Data S1 and S2).

Next, we performed GO enrichment analysis where the 1501 specific DEGs were classified into different categories according to the GO terms for biological processes. The top significant GO terms were associated with regulation of broad biological and cellular processes, localization, and nervous system development (Figure 3H,I, Data S3). In addition, numerous GO terms involving cell cycle regulation were enriched, as were axonogenesis, axon ensheathment, and myelination (Data S3).

Further, the core analysis by IPA predicted that the top canonical pathways activated in OPN-KO mice compared to control mice included ErbB and neuregulin (NRG) signaling pathways (Figure 4A, Data S3). The ErbB-NRG receptor-ligand signaling is involved in nervous system development and in the control of oligodendrocyte development and myelination.^{38,39} Other pathways predicted to be activated were apelin signaling, involved in various physiological processes including oligodendrocyte development and myelination,⁴⁰ and NF- κ B signaling, involved in many cellular pathways including cell cycle control and oligodendrocyte function. The G2/M checkpoint

regulation was predicted to be activated while cell cycle control of chromosomal replication was predicted to be inhibited, indicating a decrease of cell cycle progress and an increase of the S phase, as predicted in the biological function analysis (Figure 3A). Additionally, Rac signaling relevant to cell shape changes during oligodendrocyte development was predicted to be inhibited.

KEGG pathway analysis also revealed a high enrichment in cell cycle and ErbB signaling, as well as apoptosis, MAPK signaling, and PI3K-Akt signaling (Figure 4B), all of which are important in oligodendrocyte function by regulating cell cycle, cell survival, cell movements, development, and myelination.

Lastly, IPA suggested transcription factor 7-like 2 (TCF7L2) as the top upstream regulator activated and the prostaglandin E receptor 2 (PTGER2) to be the top upstream regulator inhibited in the OPN-KO versus control dataset (Figure 4C,D, Data S3).

Together, these analyses suggest that the main biological processes enriched in oligodendrocytes of OPN-KO mice are associated with myelination and cell cycle control.

3.4 | Oligodendrocyte-specific expression of iOPN in global absence of both isoforms alters expression of genes involved in cell adhesion and migration, vascular development, and neuronal development

To examine the effect of expression of iOPN in oligodendrocytes without the influence of sOPN, we focused on the 905 DEGs specific in OLS-iOPN-KI mice compared to control mice (Figure 2B). Of these, the top 20 upregulated genes were associated with cell movements such as actin cytoskeleton organization, focal adhesion, and migration (*Fgd5*, *Cdc42ep3*, *Nrep*, *Tgm2*, *Clec14a*, *Tm4sf1*, *Thbs2*, *Rhoj*, and *Emcn*) and lipid metabolism (*Atp10d* and *Apod*). Moreover, some of the most upregulated genes were associated with angiogenesis (*Vwf*, *Clec14a*, *Emcn*, *Tek*, and *Hspa12b*) (Table S3). The top 19 downregulated genes were linked to neuronal functions (*Stac3*, *Tenm2*, and *Camkv*), DNA damage control, and repair (*Eya4*, *Palb2*, and *Nabp1*), as well as cell proliferation and differentiation (*Trim14*, *Bmp2k*, *Hs6st3*, and *Efcab7*) (Table S4).

IPA core analysis of the 905 specific DEGs demonstrated that the top 15 increased functions in OLS-iOPN-KI mice were associated with cell movements, survival, and growth, as well as angiogenesis and vasculogenesis. Predicted decreased biological functions were mainly associated with death, apoptosis, and necrosis (Figure 5A, Data S4).

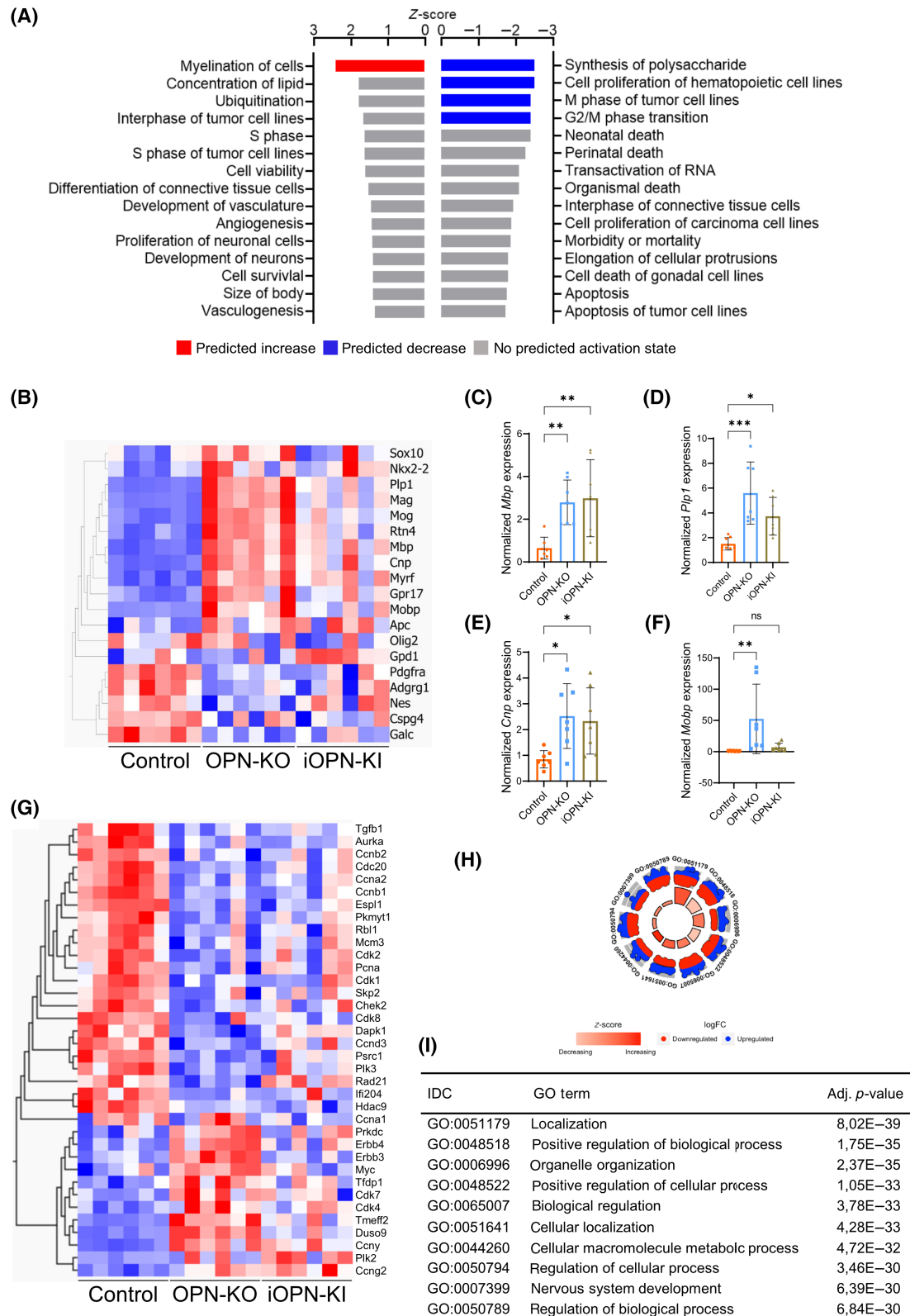


FIGURE 3 Myelination of cells and cell cycle control were predicted to be enriched biological functions in oligodendrocytes of OPN-KO mice. IPA and GO analysis were performed using the 1501 DEGs in OPN-KO versus control. (A) Histogram of the 15 most significantly enriched biological functions with most positive and most negative z-scores predicted by IPA. (B) Heatmap across all the samples using genes involved in oligodendrocyte development and myelination. (C–F) Expression analysis of the oligodendrocyte and myelin-related genes *Mbp* (C), *Plp1* (D), *Cnp* (E), and *Mobp* (F), using RT-PCR. One-way ANOVA and Dunnett's post hoc test were performed. (G) Heatmap across all the samples using genes involved in cell cycle. (H) GOplot of the most significant enriched biological processes in OPN-KO versus control. The outer circle represents how many genes that are upregulated or downregulated in the GO term. The inner circle has a double function: the height of the bar indicates negative \log_{10} of adjusted *p*-value and the color of the bar represents the z-score. (I) The GO terms. **p* < 0.05; ***p* < 0.01; ****p* < 0.001.

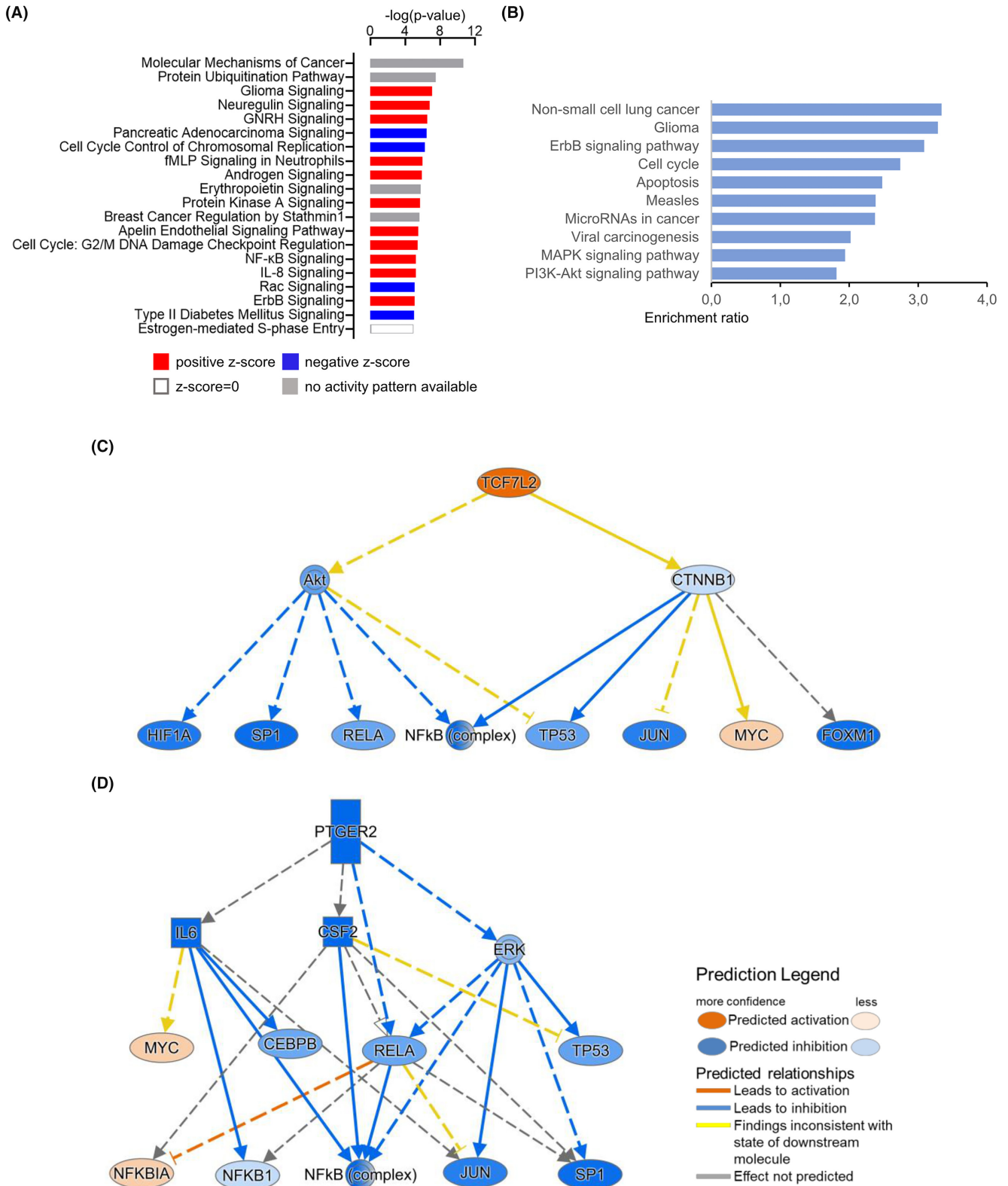


FIGURE 4 Pathway analysis revealed enriched NRG-ErbB signaling, cell cycle, and cell survival signaling in oligodendrocytes of OPN-KO mice. Canonical pathways and biological implications were assessed using IPA and KEGG pathway analysis of the 1501 DEGs in OPN-KO versus control. (A) Histogram of the 20 most significant canonical pathways predicted by IPA. (B) Top biological implications using KEGG pathway analysis. (C, D) Graphical summary of the networks predicted by IPA downstream of TCF7L2 in (C) and downstream of PTGER2 in (D).

GO analysis reinforced these findings with the top significant GO terms including developmental processes, especially the development of the vasculature, as well as cellular motility and migration (Figure 5B,C, Data S4). Further, significant enrichment was identified for several GO terms involved in the regulation of cell death, axon guidance, as well as axon and neuronal development (Data S4).

The canonical pathways from IPA (Figure 6A, Data S4) predicted to be activated included GP6 signaling pathway, nitric oxide signaling, VEGF signaling, and endothelial nitric oxide synthase (eNOS) signaling, which are all involved in vascular regulation. In addition, PI3K-Akt and mTOR signaling were activated, as well as downstream translational control pathways (eIF4-p70S6K signaling and EIF2 signaling), while its negative counterpart PTEN signaling was inhibited. Also predicted to be activated were ephrin receptor signaling involved in axon guidance, cell migration, and axon-oligodendrocyte interactions preceding myelination.⁴¹ Further, PAK signaling was predicted to be activated, which is involved in cell migration, proliferation, survival, and neuronal plasticity via its activities in actin cytoskeleton modulation.⁴² RhoGDI signaling, which negatively regulates Rho GTPases and is involved in cytoskeletal dynamics and cell movements, was predicted to be inhibited. Furthermore, KEGG pathway analysis demonstrated an enrichment in focal adhesions,

extracellular matrix (ECM)-receptor interactions, and PI3K-Akt signaling, further implicating the enrichment of cell migration and survival (Figure 6B).

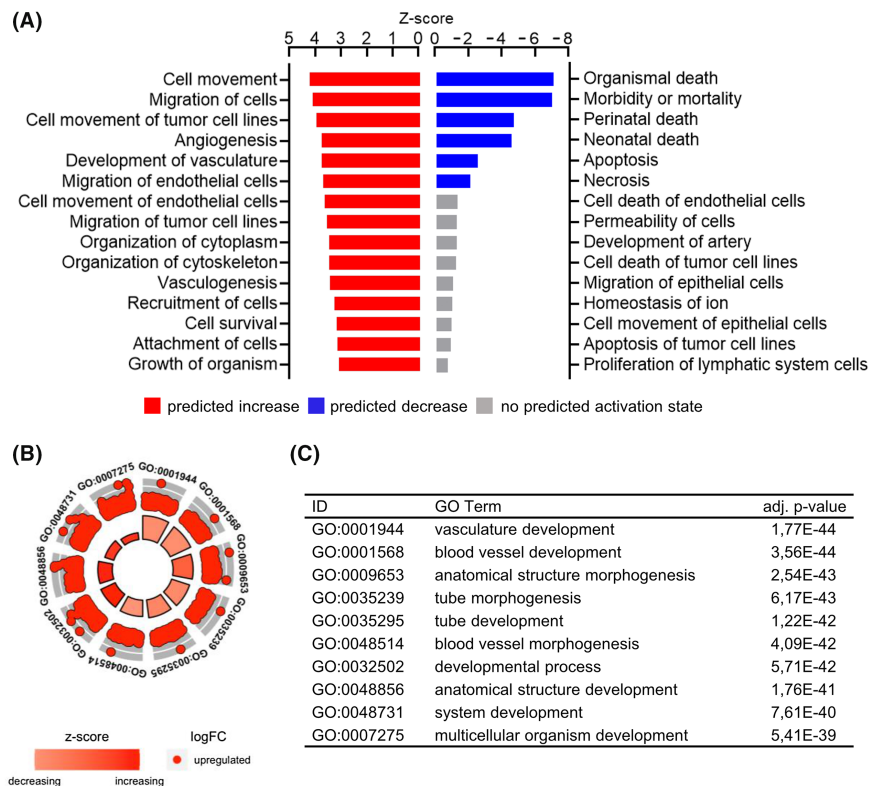
Lastly, IPA suggested the NF- κ B (complex) as the top upstream regulator activated and α -catenin (CTNNA1) as the top upstream regulator inhibited in the OLS-iOPN-KI versus control dataset (Figure 6C,D, Data S4).

Taken together, these analyses suggest that the main processes enriched in oligodendrocytes expressing iOPN, in global absence of sOPN, are associated with various aspects of cell adhesion and motility, axonal and neuronal development, and the development of brain vasculature.

3.5 | Oligodendrocyte-specific expression of iOPN in global absence of both isoforms detains continued myelin wrapping in the early phase of myelination

Next, we explored the impact of the differential expression of the two OPN isoforms in myelination in vivo. We used mice at P12, a developmental stage at which myelination has commenced, but the most rapid phase of myelination in the corpus callosum white matter has not yet begun.⁴³ TEM was used to investigate the myelin ultrastructure in the corpus callosum (Figure 7A).

FIGURE 5 Biological functions associated with cellular movements and vascular development were upregulated in OLS-iOPN-KI mice. IPA and GO analysis were performed using the 905 DEGs in OLS-iOPN-KI versus control. (A) Histogram of the 15 most significantly enriched biological functions with most positive and most negative z-scores predicted by IPA. (B) GOplot of the most significantly enriched biological processes in OLS-iOPN-KI versus control. The outer circle represents how many genes that are upregulated or downregulated in the GO term. The height of the bar in the inner circle indicates negative \log_{10} of adjusted p -value and the color of the bar represents the z-score. (C) The GO terms.



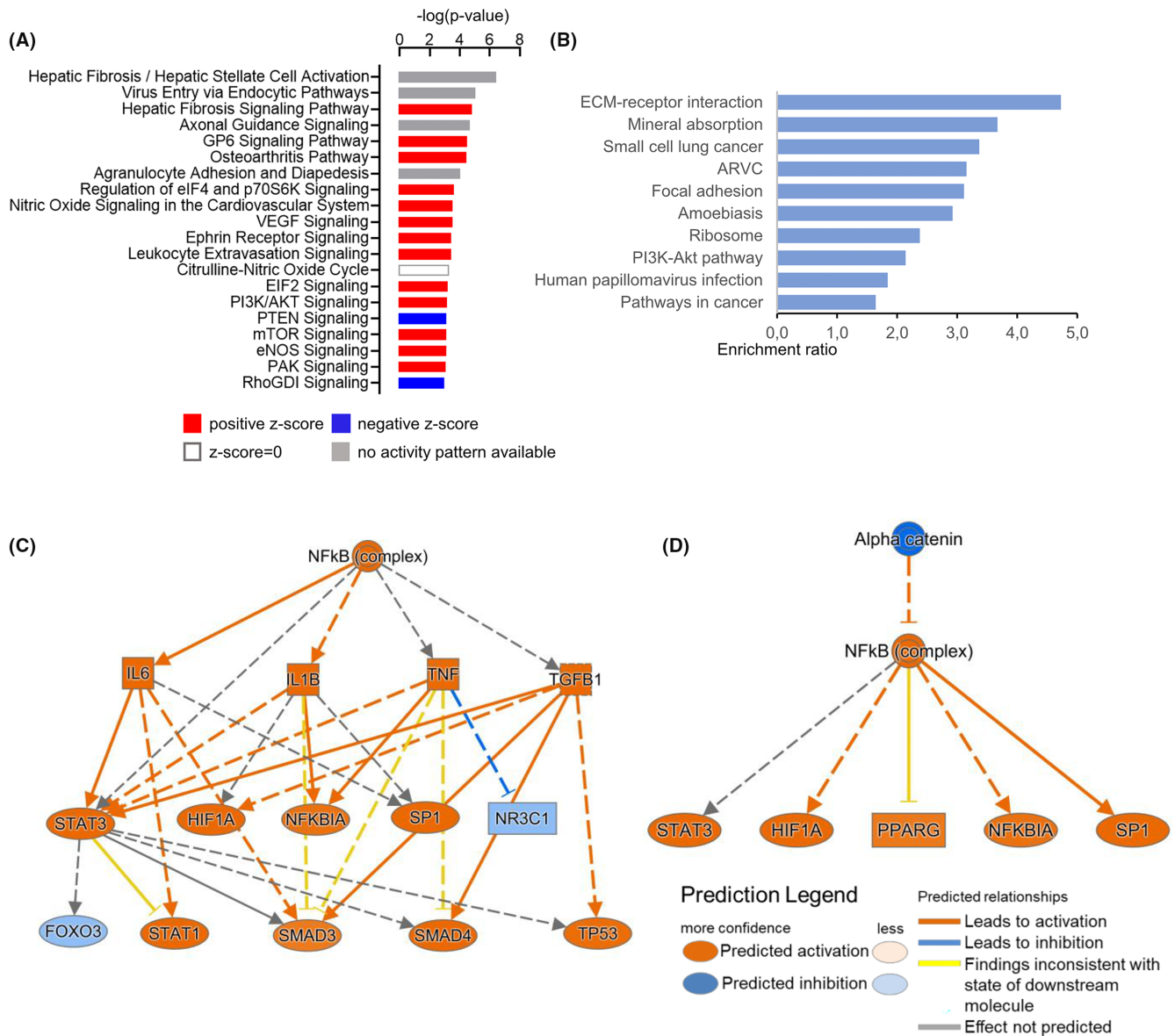
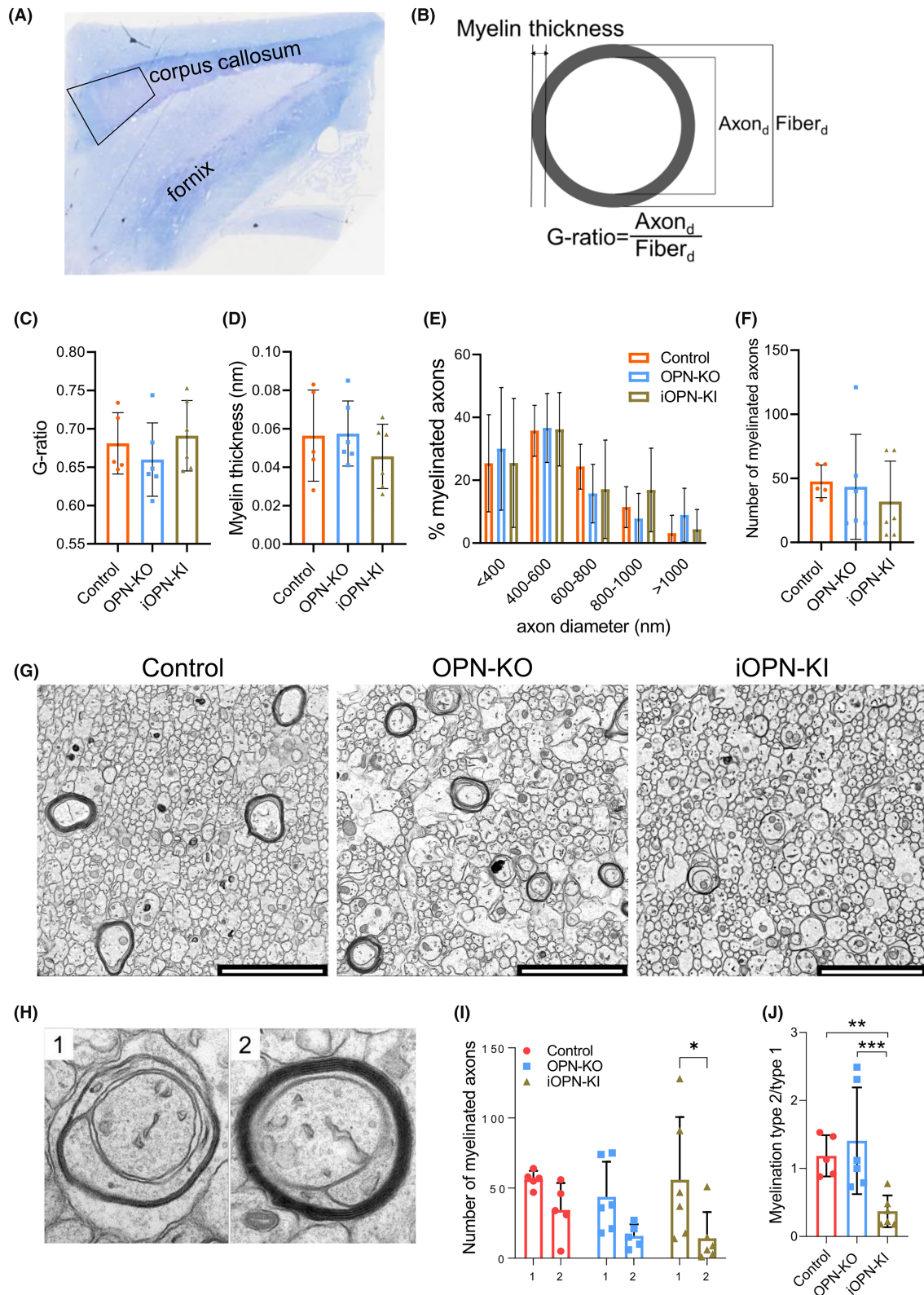


FIGURE 6 Pathways regulating cell adhesion, migration, and survival were enriched in OLS-iOPN-KI mice. Canonical pathways and biological implications were assessed using IPA and KEGG pathway analysis of the 905 DEGs in OLS-iOPN-KI versus control. (A) Histogram of the 20 most significant canonical pathways predicted by IPA. (B) Top biological implications using KEGG pathway analysis. (C, D) Graphical summary of the networks predicted by IPA downstream of NF- κ B (complex) in (C) and downstream of α -catenin in (D).

The g-ratio, a key measure of myelination defined as the ratio of the inner axonal diameter to the total outer fiber diameter (Figure 7B), was not significantly different between control, OPN-KO, and OLS-iOPN-KI mice (Figure 7C). Additionally, no significant differences were observed in myelin thickness, distribution of axon diameters, or number of myelinated axons (Figure 7D–F). However, myelination in OLS-iOPN-KI mice appeared less developed compared to control and OPN-KO mice (Figure 7G). This prompted us to further examine the degree of myelination, with type 1 axons

just being ensheathed or containing one to two myelin wraps, and type 2 axons having formed myelin sheaths (Figure 7H).

Overall, there was no significant difference between type 1 and type 2 myelination in control and OPN-KO mice, while OLS-iOPN-KI mice had significantly fewer axons with more advanced type 2 myelination compared to type 1 axons ($p=0.02$) (Figure 7I). Accordingly, the type 2:type 1 ratio was significantly reduced compared to control ($p=0.002$) and OPN-KO ($p=0.0008$) (Figure 7J). As the number of type 1 myelinated axons was similar



among the three genotypes, these results thus suggested that initiation of myelination in OLS-iOPN-KI mice was normal but continued myelin wrapping was hampered,

indicating that expression of iOPN in oligodendrocytes without sOPN might specifically inhibit the reinforcement of myelination at this stage of development.

FIGURE 7 OLS-iOPN-KI mice featured delayed myelination. Myelination in the corpus callosum was examined in control, OPN-KO, and OLS-iOPN-KI mice at P12 using TEM. (A) A representative image of a sagittal semi-thin section stained with Richardson's stain. The trapezoid shows the region that was cut into ultra-thin sections and imaged with TEM. (B) Schematic representation of an axon illustrating the measurement of myelin thickness and g-ratio calculation. Myelination was quantified by measuring g-ratio (C), myelin thickness (D), and the distribution of the diameter of myelinated axons (E). (F) The number of myelinated axons in different genotypes of mice. (G) Representative electron photomicrographs from control, OPN-KO, and OLS-iOPN-KI mice. (H) Representation of myelin wrapping classification: type 1 included axons that were ensheathed to axons with 1–2 myelin wraps, and type 2 included axons with a formed myelin sheath. (I) The number of myelinated axons of the different myelination types. (J) The ratio of myelination type 2:type 1 in the three genotypes. One-way ANOVA and Tukey's post hoc test were performed (C, D, F, J). Two-way ANOVA and Šidák's multiple comparison test were used (I). The calculations were performed on six images per animal acquired at 2000× magnification and an average of 40 axons per animal, $n = 5\text{--}6/\text{group}$. Scale bars = 3 μm . * $p < 0.05$; ** $p < 0.01$; *** $p < 0.001$.

3.6 | The lack of sOPN enhances myelination in adulthood, while oligodendrocyte-specific expression of iOPN in global absence of sOPN impairs axon integrity

Next, we explored the influence of OPN isoforms on myelination in vivo after the myelination process is completed. To this end, we used adult mice at the age of 12 weeks and used TEM to investigate the myelin ultrastructure in the corpus callosum white matter (Figure 7A,B). In contrast to young mice, the g-ratio was decreased in adult OPN-KO mice compared to controls ($p = 0.007$), but not in OLS-iOPN-KI mice compared to controls ($p = 0.35$) (Figure 8A). Furthermore, there was a significant increase of myelin thickness in both OPN-KO mice ($p = 0.0001$) and OLS-iOPN-KI mice ($p = 0.003$) while no significant difference between OLS-iOPN-KI and OPN-KO mice was observed ($p = 0.12$) (Figure 8B). The lower g-ratio in OPN-KO mice resulted from the increased myelin thickness, as the distribution of axon diameters did not differ between the genotypes (Figure 8C). Interestingly, OLS-iOPN-KI mice, but not OPN-KO and control mice, had many dark axons with dense axoplasm accompanied by collapsed myelin sheaths, which can be a characteristic of ongoing degeneration⁴⁴ (Figure 8D,E). In addition, OPN-KO and OLS-iOPN-KI mice had increased expression of the myelin-related proteins myelin basic protein (MBP) and myelin proteolipid protein 1 (PLP1) compared to control mice, assessed by western blot (Figure 8F,G).

In sum, these results suggested that sOPN may act as a negative regulator of myelination in the final stages of myelination that may involve regulation of the expression of myelin-related proteins, as increased myelin thickness and increased expression of the major constituents of myelin was observed in OPN-KO and OLS-iOPN-KI mice, which both lack the sOPN isoform. Importantly, the expression of OLS-iOPN in the absence of sOPN resulted in disruption of axonal integrity suggesting that expression of sOPN and iOPN need to be balanced for proper myelination and axonal integrity.

4 | DISCUSSION

In the current study, we used a newly generated mouse model with oligodendrocyte-specific expression of iOPN to reveal that both sOPN and OLS-iOPN isoforms are required for proper myelination and axon integrity (Figure 9). OLS-iOPN-KI mice, in which oligodendrocytes express iOPN alone without modulation by sOPN, featured delayed myelination in young age, and degenerated axons in adulthood. Oligodendrocytes from these mice showed transcriptional changes related to cell contacts, suggesting that iOPN might be involved in the communication of oligodendrocytes to the extracellular matrix and to axons, interactions important for proper myelination and axon integrity. In OPN-KO mice, lacking both sOPN and iOPN globally, and in OLS-iOPN-KI mice, increased myelination was observed in adulthood, suggesting that sOPN possibly acts as a negative regulator of myelination, and that loss of sOPN may alter myelin homeostasis. This study thus shows a separate contribution of the two OPN isoforms to myelination and axon integrity.

RNA-seq analysis of oligodendrocytes at P5, the stage during which OPN expression peaks in the mouse brain, agreed with the myelin structural observations that in the complete absence of both OPN isoforms there was an up-regulation of genes associated with myelination and IPA predicted an increase in myelination of cells. ErbB and NRG signaling that are implicated in myelination were predicted to be increased in these mice. In vitro studies have suggested that NRG-ErbB signaling is important for oligodendrocyte generation and development,^{45,46} and loss of ErbB signaling leads to hypomyelination in vivo.³⁹ In the absence of ErbB2, oligodendrocytes fail to undergo terminal differentiation and to ensheath axons.⁴⁷ Increased activation of NRG-ErbB signaling in OPN-KO mice may enhance axon myelination.

Furthermore, bioinformatic analyses predicted increased S phase with a decrease of the G2/M phase transition and M phase in OPN-KO oligodendrocytes. Consistently, several signal transduction pathways were

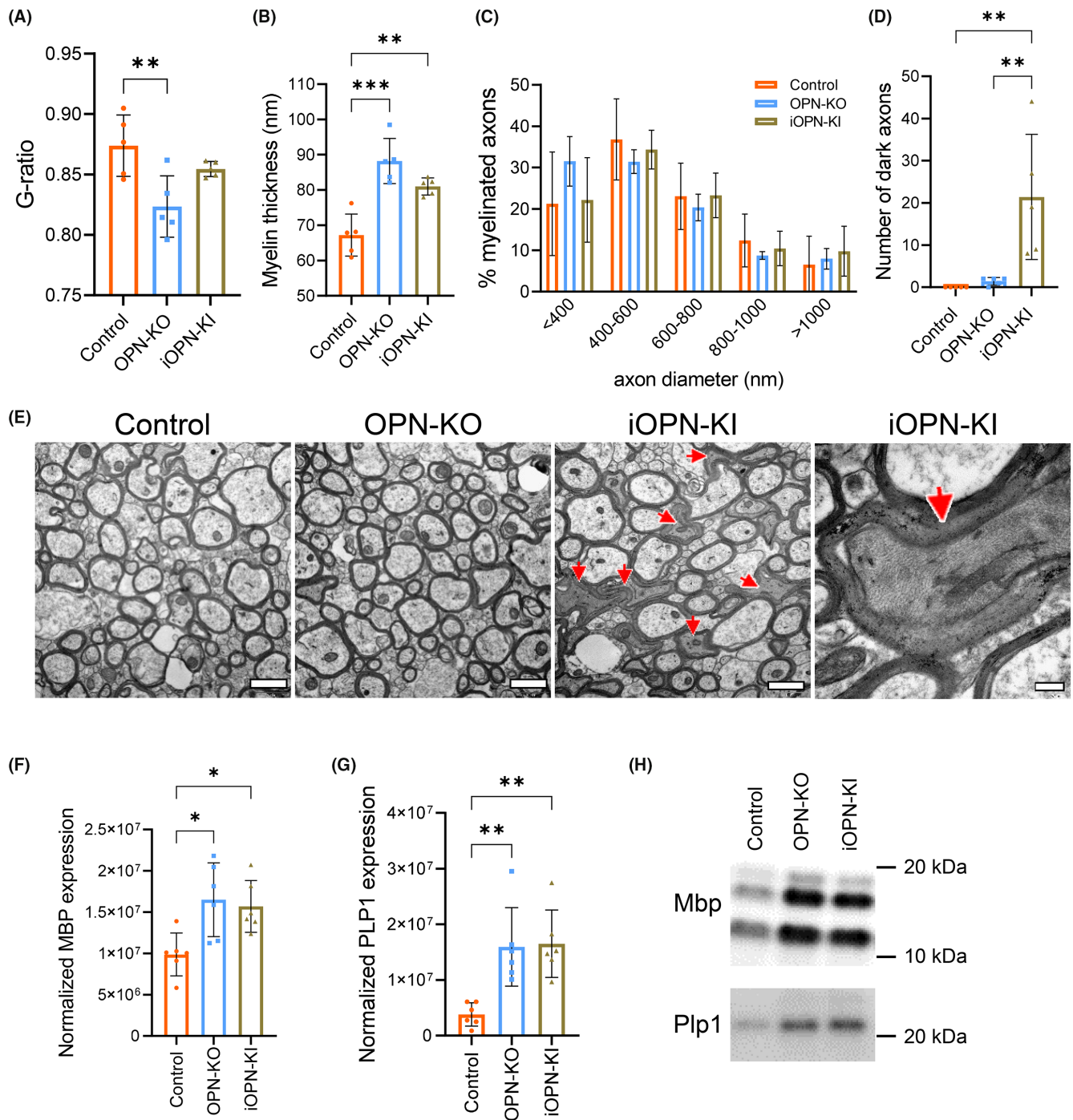


FIGURE 8 Lack of both SOPN and iOPN resulted in hypermyelination in the adult mouse brain. Myelination in the corpus callosum was examined in control, OPN-KO, and OLS-iOPN-KI 12 weeks old mice using TEM. (A–C) Morphometric data on the g-ratio (A), myelin thickness (B), and the distribution of the diameter of myelinated axons (C). (D) The number of dark axons in the different genotypes of mice. An average of 300 axons/mouse was counted, $n = 5$ /group. One-way ANOVA and Tukey's post hoc test were performed (A, B, D). (E) Representative electron micrographs showing myelinated axons in the different genotypes of mice (left three panels, 12,500× magnification, scale bar = 1000 nm), and dark axons (red arrows) in OLS-iOPN-KI mice (the panel on the far right, 50,000× magnification, scale bar = 200 nm). (F, G) Expression analysis of the myelin-related proteins MBP (F) and PLP1 (G) using western blot. MBP and PLP1 expression were normalized to total protein levels. One-way ANOVA and Dunnett's post hoc test were performed. (H) Representative western blot images of MBP (upper panel) and PLP1 (lower panel). * $p < 0.05$; ** $p < 0.01$; *** $p < 0.001$.

predicted to be altered in OPN-KO cells, which could be involved in the dysregulation of cell cycle control, including NF- κ B signaling and the PI3K-Akt pathway.

TCF7L2 (also called TCF4) was predicted to be the top activated upstream regulator in OPN-KO oligodendrocytes compared to controls. TCF7L2 is a transcription factor and

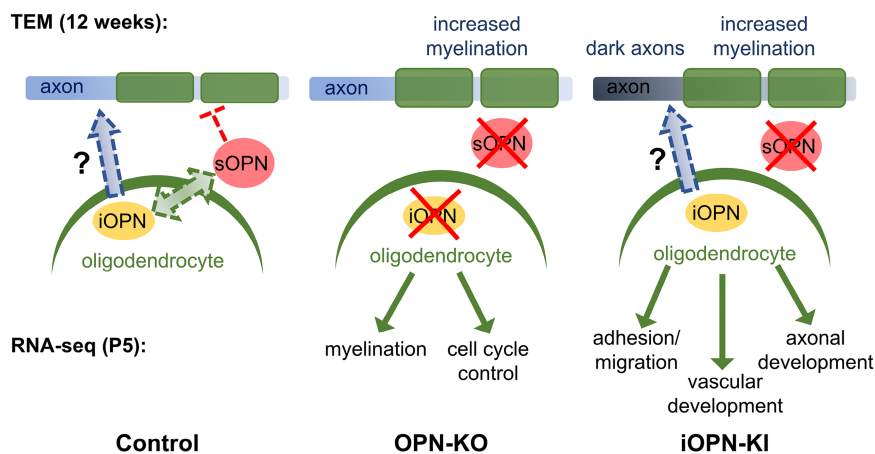


FIGURE 9 Schematic summary. During normal conditions (control, left panel) sOPN and OLs-iOPN contribute to a proper myelination process and axonal integrity, where sOPN possibly act as a negative regulator of myelination in the final stages of myelination. iOPN may have a role in the contact of oligodendrocytes to the external environment, which could involve sOPN interplay, and/or axon contact, interactions important for myelination and axon integrity. The absence of both isoforms (OPN-KO, middle panel) leads to an increase of myelination at adulthood and transcriptomic changes related to increased myelination genes and signaling already at early age. OLs-iOPN expression without modulation by sOPN (iOPN-KI, right panel), resulted in an increased myelination as well as dark axoplasm and signs of axon degeneration in adulthood, and transcriptomic changes in oligodendrocytes at early age included enrichment of genes and pathways related to cell adhesion/migration and axonal development.

a key mediator of the canonical Wnt pathway that is expressed in oligodendrocytes only in early postnatal stages where it is required for oligodendrocyte development and myelination.^{48,49} PTGER2, which was predicted to be the top upstream inhibited regulator, has been shown to arrest oligodendrocyte progenitor maturation.⁵⁰ However, whether the regulation by these factors is involved in the hypermyelination observed in the absence of both isoforms of OPN warrants further investigations.

While a complete loss of OPN resulted in an increased myelination, the expression of OLs-iOPN in the absence of sOPN primarily affected functions and pathways involved in actin cytoskeleton arrangements, cell adhesion, and cell migration. In OLs-iOPN-KI mice, the expression of iOPN in oligodendrocytes in the absence of sOPN interfered with myelination at P12, when myelination begins.⁴³ Specifically, in these mice, initial axon ensheathment was normal but myelin wrapping was delayed. Axon ensheathment by oligodendrocytes and subsequent myelin wrapping are proposed to be driven by Arp2/3-dependent actin filament assembly followed by actin filament disassembly through the interactions of PI (4, 5) P2 with cofilin and gelsolin.^{51,52} sOPN is known to bind to the CD44 receptor,⁵³ which is expressed by oligodendrocyte precursors (OPCs) at early postnatal stages,⁵⁴ while iOPN is found to be colocalized with CD44⁵⁵ to modulate CD44 activities⁵⁶ and regulate cell protrusion and migration as part of the CD44-ezrin/radixin/moesin (ERM) complex.⁸ Moreover, the ERM complex interacts with PI (4, 5) P2 to link actin filaments to the cell membrane.⁵⁷ In addition, sOPN activates PI (4, 5) P2 and the

association of Arp2/3 with WASP, thus inducing actin polymerization.⁵⁸ Indeed, the fact that genes involved in actin cytoskeleton organization are among the top up-regulated genes in OLs-iOPN-KI mice further reinforces the possible link between the two OPN isoforms, actin organization, and myelination. Furthermore, the alteration of actin dynamics may also affect microtubule and neurofilament organization within the axons,⁵⁹ resulting in condensed electron dense axoplasm,^{60,61} which may at least partly explain the dark axons observed in adult OLs-iOPN-KI mice.

The different outcomes in the OPN-KO and OLs-iOPN-KI mouse models may be at least in part attributed to differential activity of the MAPK pathway and PI3K-Akt pathway in OPN-KO and OLs-iOPN-KI mice, respectively. Both the MEK/ERK1/2-MAPK and PI3K/Akt/mTOR signaling pathways play important roles in the regulation of myelination, and they cooperate to promote myelin sheath growth.⁶² PI3K-Akt promotes oligodendrocyte development and initiation of myelination through mTOR complex 1 (mTORC1), while MEK-ERK1/2-MAPK preserves the integrity of myelinated axons in adulthood independently of mTORC1. The above molecular pathways and networks might act in concert to regulate axon myelination and integrity, leading to the upregulation of myelination-related genes in OPN-KO oligodendrocytes already at early developmental stages.

IPA and GO analysis indicated an activation of pathways involved in the vasculature development in OLs-iOPN-KI oligodendrocytes, including nitric oxide, VEGF, and eNOS

signaling. VEGF signaling regulates OPC migration⁶³ and OPCs migrate extensively during development using the vasculature as a physical substrate.⁶⁴ OPC HIF α signaling has been suggested to couple postnatal white matter angiogenesis, axon integrity, and the onset of myelination,³⁷ and oligodendroglial HIF α has been shown to activate VEGF and regulate CNS angiogenesis.⁶⁵ *Hif1a* was upregulated in OLS-iOPN-KI mice and HIF α signaling was among the predicted canonical pathways, thus providing a potential link between iOPN, angiogenesis, and myelination. However, future studies are required to better understand the possible involvement of iOPN in angiogenesis. A limitation of the study is that further investigations of whether sOPN and OLS-iOPN share similar molecular pathways or regulate distinct gene networks to impact oligodendrocyte development, myelination, and axon integrity were not carried out but lie in the future studies.

In summary (Figure 9), here we show that iOPN and sOPN have distinct but likely interacting functions during myelination. In the absence of sOPN, OLS-iOPN has a negative effect on myelination during the initiation stages, and subsequently, the axon integrity, while genetic ablation of both isoforms rescues this effect. In adulthood, sOPN acted as a negative regulator of myelination, demonstrating that effects differ between developmental stages, which might explain the contradictory results regarding the role of OPN in white matter injury and disease, neurodegeneration, and neuroprotection in developing and adult brains.

AUTHOR CONTRIBUTIONS

Xiaoyang Wang, Jianmei W. Leavenworth, Gisela Nilsson, and Amin Mottahedin conceived and designed the research. Gisela Nilsson, Aura Zelco, Juan Song, C. Joakim Ek, Sha Hua, and Xiaoli Zhang performed and analyzed the experiments. Gisela Nilsson, Maryam Ardalán, and Xiaoli Zhang performed the statistical analysis. Volker M. Lauschke, Amin Mottahedin, C. Joakim Ek, Aura Zelco, and Gisela Nilsson carried out the bioinformatic analyses. Gisela Nilsson, Xiaoyang Wang, and Jianmei W. Leavenworth wrote the manuscript. Amin Mottahedin, Volker M. Lauschke, Carina Mallard, and Henrik Hagberg revised the manuscript critically for important intellectual content. All authors contributed to data interpretation and the revision of the manuscript and approved the submitted version.

ACKNOWLEDGMENTS

Anna-Lena Leverin and Pernilla Svedin at the Institute of Physiology and Neuroscience at the University of Gothenburg, and Daniel Caj Christie from the University of Sydney provided technical support. The Bioinformatics Core Facility and Center for Cellular Imaging at the

University of Gothenburg assisted in RNA-sequencing data processing and transmission electron microscopy, respectively. Michael Krüer from the University of Arizona College of Medicine Phoenix, Yiran Xu at Zhengzhou University, Brad Zuchero at Stanford University, Harvey Cantor and Xianli Shen from Dana-Farber Cancer Institute, Harvard Medical School, provided valuable scientific discussions.

FUNDING INFORMATION

This work was supported by the Swedish Research Council (2015-06276, 2018-02682, and 2021-01950 to XW; 2019-01320 to HH; 202101872 to CM), the Brain Foundation (FO2017-0102 to XW; FO2019-0056 to HH), Grants from the Swedish state under the agreement between the Swedish Government and the county councils, the ALF-agreement (ALFGBG-429801, ALFGBG-813291, and ALFGBG-966034 to XW; ALFGBG-432291 to HH; ALFGBG-966107 to CM), the National Natural Science Foundation of China (81771418 to XW); W o M Lundgren (1320-2016, 1804-2017, and 3126-2019 to GN), Castegrens minne (LA2016-0404 to GN), Goljes minne (LA2015-0255 to GN), Mary von Sydow (4617 and 3618 to GN), Åhlénstiftelsen (193054 and mH3h18 to GN), and the Elisabeth “Bollan” Lindén scholarship (to GN). Lauschke VM acknowledges support from the Swedish Research Council (2016-01153, 2016-01154 and 2019-01837), the Swedish Strategic Research Programme in Diabetes (SFO Diabetes), and Stem Cells and Regenerative Medicine (SFO StratRegen). XZ was supported by the Chinese Scholarship Council (201407040032), and JS was supported by funding from the Health Commission of Henan Province (2018069) and the Henan Administration of Foreign Experts Affairs (2019023) China.

DISCLOSURES

VML is a founder, CEO, and shareholder of HepaPredict AB. In addition, VML discloses consultancy work for EnginZyme AB. The authors have no additional financial interests.

DATA AVAILABILITY STATEMENT

The data that support the findings of this study are available in the methods and/or supplementary material of this article.


ORCID

Gisela Nilsson  <https://orcid.org/0000-0003-4423-5082>

Amin Mottahedin  <https://orcid.org/0000-0002-3677-2198>

Aura Zelco  <https://orcid.org/0000-0002-3677-2198>

Aura Zelco  <https://orcid.org/0000-0002-5851-6355>

Volker M. Lauschke  <https://orcid.org/0000-0002-1140-6204>

Volker M. Lauschke  <https://orcid.org/0000-0002-1140-6204>

C. Joakim Ek  <https://orcid.org/0000-0002-5764-7679>
 Maryam Ardalan  <https://orcid.org/0000-0003-3414-1584>
 Xiaoli Zhang  <https://orcid.org/0000-0001-5111-9405>
 Carina Mallard  <https://orcid.org/0000-0001-8953-919X>
 Henrik Hagberg  <https://orcid.org/0000-0003-3962-1448>
 Jianmei W. Leavenworth  <https://orcid.org/0000-0002-4100-9883>
 Xiaoyang Wang  <https://orcid.org/0000-0001-9717-8160>

REFERENCES

- Back SA, Luo NL, Borenstein NS, Levine JM, Volpe JJ, Kinney HC. Late oligodendrocyte progenitors coincide with the developmental window of vulnerability for human perinatal white matter injury. *J Neurosci*. 2001;21:1302-1312.
- Denhardt DT, Noda M, O'Regan AW, Pavlin D, Berman JS. Osteopontin as a means to cope with environmental insults: regulation of inflammation, tissue remodeling, and cell survival. *J Clin Invest*. 2001;107:1055-1061.
- Lund SA, Giachelli CM, Scatena M. The role of osteopontin in inflammatory processes. *J Cell Commun Signal*. 2009;3:311-322.
- Wang KX, Denhardt DT. Osteopontin: role in immune regulation and stress responses. *Cytokine Growth Factor Rev*. 2008;19:333-345.
- Rittling SR, Singh R. Osteopontin in immune-mediated diseases. *J Dent Res*. 2015;94:1638-1645.
- Zohar R, Lee W, Arora P, Cheifetz S, McCulloch C, Sodek J. Single cell analysis of intracellular osteopontin in osteogenic cultures of fetal rat calvarial cells. *J Cell Physiol*. 1997;170:88-100.
- Shinohara ML, Kim HJ, Kim JH, Garcia VA, Cantor H. Alternative translation of osteopontin generates intracellular and secreted isoforms that mediate distinct biological activities in dendritic cells. *Proc Natl Acad Sci USA*. 2008;105:7235-7239.
- Zohar R, Suzuki N, Suzuki K, et al. Intracellular osteopontin is an integral component of the CD44-ERM complex involved in cell migration. *J Cell Physiol*. 2000;184:118-130.
- Leavenworth JW, Verbinnen B, Yin J, Huang H, Cantor H. A p85alpha-osteopontin axis couples the receptor ICOS to sustained Bcl-6 expression by follicular helper and regulatory T cells. *Nat Immunol*. 2015;16:96-106.
- Zhao K, Zhang M, Zhang L, et al. Intracellular osteopontin stabilizes TRAF3 to positively regulate innate antiviral response. *Sci Rep*. 2016;6:23771.
- Kanayama M, Xu S, Danzaki K, et al. Skewing of the population balance of lymphoid and myeloid cells by secreted and intracellular osteopontin. *Nat Immunol*. 2017;18:973-984.
- Shinohara ML, Kim JH, Garcia VA, Cantor H. Engagement of the type I interferon receptor on dendritic cells inhibits T helper 17 cell development: role of intracellular osteopontin. *Immunity*. 2008;29:68-78.
- Inoue M, Shinohara ML. Intracellular osteopontin (iOPN) and immunity. *Immunol Res*. 2011;49:160-172.
- Cantor H, Shinohara ML. Regulation of T-helper-cell lineage development by osteopontin: the inside story. *Nat Rev Immunol*. 2009;9:137-141.
- Yang H, Ye X, Zhang X, Li X, Fu Q, Tang Z. Intracellular osteopontin negatively regulates toll-like receptor 4-mediated inflammatory response via regulating GSK3beta and 4EBP1 phosphorylation. *Cytokine*. 2018;108:89-95.
- Inoue M, Shinohara ML. Cutting edge: role of osteopontin and integrin alpha v in T cell-mediated anti-inflammatory responses in endotoxemia. *J Immunol*. 2015;194:5595-5598.
- Comi C, Carecchio M, Chiochetti A, et al. Osteopontin is increased in the cerebrospinal fluid of patients with Alzheimer's disease and its levels correlate with cognitive decline. *J Alzheimers Dis*. 2010;19:1143-1148.
- Rentsendorj A, Sheyn J, Fuchs DT, et al. A novel role for osteopontin in macrophage-mediated amyloid-beta clearance in Alzheimer's models. *Brain Behav Immun*. 2018;67:163-180.
- Albertsson AM, Zhang X, Leavenworth J, et al. The effect of osteopontin and osteopontin-derived peptides on preterm brain injury. *J Neuroinflammation*. 2014;11:197.
- Chen W, Ma Q, Suzuki H, Hartman R, Tang J, Zhang JH. Osteopontin reduced hypoxia-ischemia neonatal brain injury by suppression of apoptosis in a rat pup model. *Stroke*. 2011;42:764-769.
- van Velthoven CT, Heijnen CJ, van Bel F, Kavelaars A. Osteopontin enhances endogenous repair after neonatal hypoxic-ischemic brain injury. *Stroke*. 2011;42:2294-2301.
- Hedtjarn M, Mallard C, Hagberg H. Inflammatory gene profiling in the developing mouse brain after hypoxia-ischemia. *J Cereb Blood Flow Metab*. 2004;24:1333-1351.
- Nilsson G, Baburamani AA, Rutherford MA, et al. White matter injury but not germinal matrix hemorrhage induces elevated osteopontin expression in human preterm brains. *Acta Neuropathol Commun*. 2021;9:166.
- Tanaka F, Ozawa Y, Inage Y, et al. Association of osteopontin with ischemic axonal death in periventricular leukomalacia. *Acta Neuropathol*. 2000;100:69-74.
- Jiang R, Prell C, Lonnerdal B. Milk osteopontin promotes brain development by up-regulating osteopontin in the brain in early life. *FASEB J*. 2019;33:1681-1694.
- Selvaraju R, Bernasconi L, Losberger C, et al. Osteopontin is upregulated during in vivo demyelination and remyelination and enhances myelin formation in vitro. *Mol Cell Neurosci*. 2004;25:707-721.
- Chabas D, Baranzini SE, Mitchell D, et al. The influence of the proinflammatory cytokine, osteopontin, on autoimmune demyelinating disease. *Science*. 2001;294:1731-1735.
- Jansson M, Panoutsakopoulou V, Baker J, Klein L, Cantor H. Cutting edge: attenuated experimental autoimmune encephalomyelitis in eta-1/osteopontin-deficient mice. *J Immunol*. 2002;168:2096-2099.
- Meller R, Stevens SL, Minami M, et al. Neuroprotection by osteopontin in stroke. *J Cereb Blood Flow Metab*. 2005;25:217-225.
- Bonestroff HJ, Nijboer CH, van Velthoven CT, van Bel F, Heijnen CJ. The neonatal brain is not protected by osteopontin peptide treatment after hypoxia-ischemia. *Dev Neurosci*. 2015;37:142-152.
- du Sert NP, Hurst V, Ahluwalia A, et al. The ARRIVE guidelines 2.0: updated guidelines for reporting animal research. *PLoS Biol*. 2020;18:e3000410.
- Liao Y, Wang J, Jaehnig EJ, Shi Z, Zhang B. WebGestalt 2019: gene set analysis toolkit with revamped UIs and APIs. *Nucleic Acids Res*. 2019;47:W199-W205.
- Romero R, Espinoza J, Goncalves LF, Kusanovic JP, Friel L, Hassan S. The role of inflammation and infection in preterm birth. *Semin Reprod Med*. 2007;25:21-39.

34. Walter W, Sanchez-Cabo F, Ricote M. GOpplot: an R package for visually combining expression data with functional analysis. *Bioinformatics*. 2015;31:2912-2914.
35. Morikawa S, Sato A, Ezaki T. A simple, one-step polychromatic staining method for epoxy-embedded semithin tissue sections. *Microscopy (Oxf)*. 2018;67:331-344.
36. Lu QR, Sun T, Zhu Z, et al. Common developmental requirement for Olig function indicates a motor neuron/oligodendrocyte connection. *Cell*. 2002;109:75-86.
37. Yuen TJ, Silbereis JC, Griveau A, et al. Oligodendrocyte-encoded HIF function couples postnatal myelination and white matter angiogenesis. *Cell*. 2014;158:383-396.
38. Mei L, Nave KA. Neuregulin-ERBB signaling in the nervous system and neuropsychiatric diseases. *Neuron*. 2014;83:27-49.
39. Roy K, Murtie JC, El Khodort BF, et al. Loss of erbB signaling in oligodendrocytes alters myelin and dopaminergic function, a potential mechanism for neuropsychiatric disorders. *Proc Natl Acad Sci U S A*. 2007;104:8131-8136.
40. Quan LL, Uyeda A, Muramatsu R. Central nervous system regeneration: the roles of glial cells in the potential molecular mechanism underlying remyelination. *Inflamm Regen*. 2022;42:7.
41. Linneberg C, Harboe M, Laursen LS. Axo-glia interaction preceding CNS myelination is regulated by bidirectional Eph-ephrin signaling. *ASN Neuro*. 2015;7:175909141560285.
42. Zhang KF, Wang Y, Fan TD, Zeng C, Sun ZS. The p21-activated kinases in neural cytoskeletal remodeling and related neurological disorders. *Protein Cell*. 2022;13:6-25.
43. Sturrock RR. Myelination of the mouse corpus callosum. *Neuropathol Appl Neurobiol*. 1980;6:415-420.
44. Stassart RM, Mobius W, Nave KA, Edgar JM. The axon-myelin unit in development and degenerative disease. *Front Neurosci*. 2018;12:467.
45. Navel KA, Salzer JL. Axonal regulation of myelination by neuregulin 1. *Curr Opin Neurobiol*. 2006;16:492-500.
46. Calaora V, Rogister B, Bismuth K, et al. Neuregulin signaling regulates neural precursor growth and the generation of oligodendrocytes in vitro. *J Neurosci*. 2001;21:4740-4751.
47. Park SK, Miller R, Krane I, Vartanian T. The erbB2 gene is required for the development of terminally differentiated spinal cord oligodendrocytes. *J Cell Biol*. 2001;154:1245-1258.
48. Fancy SP, Baranzini SE, Zhao C, et al. Dysregulation of the Wnt pathway inhibits timely myelination and remyelination in the mammalian CNS. *Genes Dev*. 2009;23:1571-1585.
49. Zhao CT, Deng YQ, Liu L, et al. Dual regulatory switch through interactions of Tcf7l2/Tcf4 with stage-specific partners propels oligodendroglial maturation. *Nat Commun*. 2016;7:10883.
50. Shioh LR, Favrais G, Schirmer L, et al. Reactive astrocyte COX2-PGE2 production inhibits oligodendrocyte maturation in neonatal white matter injury. *Glia*. 2017;65:2024-2037.
51. Zuchero JB, Fu MM, Sloan SA, et al. CNS myelin wrapping is driven by actin disassembly. *Dev Cell*. 2015;34:152-167.
52. Nawaz S, Sanchez P, Schmitt S, et al. Actin filament turnover drives leading edge growth during myelin sheath formation in the central nervous system. *Dev Cell*. 2015;34:139-151.
53. Weber GF, Ashkar S, Glimcher MJ, Cantor H. Receptor-ligand interaction between CD44 and osteopontin (Eta-1). *Science*. 1996;271:509-512.
54. Naruse M, Shibasaki K, Yokoyama S, Kurachi M, Ishizaki Y. Dynamic changes of CD44 expression from progenitors to subpopulations of astrocytes and neurons in developing cerebellum. *PLoS ONE*. 2013;8:e53109.
55. Suzuki K, Zhu B, Rittling SR, et al. Colocalization of intracellular osteopontin with CD44 is associated with migration, cell fusion, and resorption in osteoclasts. *J Bone Miner Res*. 2002;17:1486-1497.
56. Zhu B, Suzuki K, Goldberg HA, et al. Osteopontin modulates CD44-dependent chemotaxis of peritoneal macrophages through G-protein-coupled receptors: evidence of a role for an intracellular form of osteopontin. *J Cell Physiol*. 2004;198:155-167.
57. Senju Y, Lappalainen P. Regulation of actin dynamics by PI(4,5)P2 in cell migration and endocytosis. *Curr Opin Cell Biol*. 2019;56:7-13.
58. Chellaiah MA. Regulation of actin ring formation by rho GTPases in osteoclasts. *J Biol Chem*. 2005;280:32930-32943.
59. Kevenaar JT, Hoogenraad CC. The axonal cytoskeleton: from organization to function. *Front Mol Neurosci*. 2015;8:44.
60. Kirkpatrick LL, Witt AS, Payne HR, Shine HD, Brady ST. Changes in microtubule stability and density in myelin-deficient shiverer mouse CNS axons. *J Neurosci*. 2001;21:2288-2297.
61. Cepurna WO, Kayton RJ, Johnson EC, Morrison JC. Age related optic nerve axonal loss in adult Brown Norway rats. *Exp Eye Res*. 2005;80:877-884.
62. Ishii A, Furusho M, Macklin W, Bansal R. Independent and cooperative roles of the Mek/ERK1/2-MAPK and PI3K/Akt/mTOR pathways during developmental myelination and in adulthood. *Glia*. 2019;67:1277-1295.
63. Hayakawa K, Pham LDD, Som AT, et al. Vascular endothelial growth factor regulates the migration of oligodendrocyte precursor cells. *J Neurosci*. 2011;31:10666-10670.
64. Tsai HH, Niu J, Munji R, et al. Oligodendrocyte precursors migrate along vasculature in the developing nervous system. *Science*. 2016;351:379-384.
65. Zhang S, Kim B, Zhu XQ, et al. Glial type specific regulation of CNS angiogenesis by HIF alpha-activated different signaling pathways. *Nat Commun*. 2020;11:2027.

SUPPORTING INFORMATION

Additional supporting information can be found online in the Supporting Information section at the end of this article.

How to cite this article: Nilsson G, Mottahedin A, Zelco A, et al. Two different isoforms of osteopontin modulate myelination and axonal integrity. *FASEB BioAdvances*. 2023;5:336-353. doi:[10.1096/fba.2023-00030](https://doi.org/10.1096/fba.2023-00030)